THE ASTROPHYSICAL JOURNAL, 419:780–792, 1993 December 20

THE SECONDARY OUTBURST MAXIMUM OF T CORONAE BOREALIS: HYDRODYNAMIC SIMULATIONS OF THE BLOB AND ACCRETION DISK

MAXIMILIAN RUFFERT
Max-Planck-Institut für Astrophysik, Postfach 1523, 85740 Garching, Germany
JOHN K. CANNIZZO[1,2]
Max-Planck-Institut für Astrophysik, Postfach 1523, 85740 Garching, Germany; and NASA/Goddard Space Flight Center, Laboratory for Astronomy and Solar Physics, Code 681, Greenbelt, MD 20771
AND
SCOTT J. KENYON
Harvard-Smithsonian Center for Astrophysics, 60 Garden Street, Cambridge, MA 02138
Received 1992 November 5; accepted 1993 May 20

ABSTRACT

We continue the investigation of Cannizzo & Kenyon into the model proposed by Webbink to account for the eruptive behavior of the recurrent nova T CrB which occurred in 1946. In particular, we present three-dimensional hydrodynamical computations of the blob of material which is ejected from the mass-losing star in the Webbink model and find that, within several dynamical timescales, the blob should become smeared out by tidal forces and internal gas pressure into a disk-shaped body with roughly constant surface density (as projected onto the orbital plane). We then reexamine the spreading torus model employed by Cannizzo & Kenyon to account for the observed secondary maximum in the 1946 outburst using a one-dimensional accretion disk model within the context of the three-dimensional hydrodynamical results. The model presented by Cannizzo & Kenyon of an exponentially increasing viscosity parameter $\alpha(t)$ for the accretion disk is still viable, but the accretion disk flux during early times is much greater than before. In addition, during the time before peak accretion disk luminosity there are two outward-moving transition fronts—one associated with the transition between the low- and high-α regions of the disk, and a second associated with the interface between ionized and neutral disk material. These are roughly coincident with each other and are caused by the outward wave of increasing accretion disk viscosity which comes about when one takes a local growth rate for α dependent on the Keplerian frequency. We are able to reproduce the secondary maximum fairly well using 10^{-5} and 3 for initial and final values of α, and a local growth timescale for α of $2/\Omega$.

Subject headings: accretion, accretion disks — hydrodynamics — stars: individual (T Coronae Borealis)

1. INTRODUCTION

T Coronae Borealis is one of several symbiotic binary stars classified as recurrent novae (Kenyon 1986: Webbink et al. 1987, hereafter WLTO). The system consists of an M3 giant primary that fills its tidal lobe and transfers matter onto a hot companion. Several dynamical mass estimates suggest the secondary exceeds the Chandrasekhar limit and must be a main-sequence star (Kenyon & Garcia 1986, hereafter KG); however, many observations—including the ultraviolet energy distribution and nova-like eruptions—appear more easily interpreted if the secondary is a white dwarf star (Selvelli et al. 1992; and references therein).

The two recorded eruptions of T CrB (1866 and 1946) have been remarkably similar. A $\sim$6–7 mag rise to visual maximum took less than 1 day in both instances, and the system returned to apparently normal minimum states in $\sim$40 days. Unlike most recurrent novae, T CrB then rose $\sim$2 mag over $\sim$30 days to a secondary optical maximum that lasted several hundred days (see Cannizzo & Kenyon 1992). Webbink (1976) proposed an accretion model for this behavior, in which the mass loser ejects a blob of matter very quickly (i.e., on less than a dynamical timescale for the primary) which travels through the $L1$ point "down" to the accreting star. The circularization of this blob into a torus of matter orbiting the accretor gives rise to the primary maximum, and its subsequent spreading into a disk and accretion onto the main-sequence (MS) star produces the secondary maximum. Cannizzo & Kenyon (1992, hereafter CK) examined the ramifications of Webbink's model by utilizing a one-dimensional model for the spreading torus of matter that forms out of the blob. They found that the short observed rise and decay times and the relatively long ($\sim$100 day) interval between primary and secondary maxima imply that the viscous dissipation within the torus/accretion disk must remain very low for many local orbital timescales and then increase abruptly. This evolution makes physical sense if the viscosity couples to the orbital shear in the disk, because the viscosity would then require a few orbital times to increase from some "seed" value in the protodisk to its saturation value.

A major shortcoming of CK's study is that the initial state of the disk was given by fiat. CK assumed that the matter in the blob circularized into a well-defined torus centered at the Lubow-Shu radius, where the Keplerian angular momentum equals that of matter at the $L1$ point (Lubow & Shu 1975). Furthermore, CK ran several models with varying initial mass, because they did not know what fraction of the initial blob

[1] Humboldt Fellow.
[2] NRC Senior Associate.

survived in the postcircularization torus. Our aim in the present work is to use a three-dimensional hydrodynamical code to follow the evolution of the blob as it becomes disrupted due to tidal forces and its own internal gas pressure, and determine (1) the degree of spreading during the ~ 100 day interval between the two observed maxima in the system and (2) the fraction of the blob that stays within the Roche volume of the accreting star. Having obtained this information, we revisit the one-dimensional disk model employed by CK and redo their computations with the more realistic initial physical parameters for the protodisk.

In § 2 we present a discussion of the two numerical methods employed and a summary of the results from each method. Section 3 attempts a synthesis of the information acquired through hydrodynamical computations for the blob and accretion disk, and § 4 sums up.

2. HYDRODYNAMICAL COMPUTATIONS

2.1. *Three-dimensional Simulations of the Spreading Blob*

2.1.1. *Input Physics*

2.1.1.1. Model Assumptions

From the binary orbital period $P \approx 227.5$ days obtained by KG, one obtains an angular velocity for the system of $\omega = 2\pi/P \approx 3.2 \times 10^{-7}$ s^{-1} and a separation

$$a = \left[\frac{G(M_1 + M_2)}{\omega^2}\right]^{1/3} \approx 1.7 \times 10^{13} \text{ cm} . \quad (1)$$

In this study we adopt the minimum masses for the two stars inferred by KG which are $M_1 = 2.1\ M_\odot$ (mass loser) and $M_2 = 1.6\ M_\odot$ (mass gainer). The position $L1$ for our mass ratio $q = M_2/M_1 \approx 0.76$ is about $0.52a$ distant from the primary (i.e., the $L1$ point is nearly in the middle).

We treat both the (primary) Roche lobe–filling star and the (secondary) mass-accreting star as gravitating point masses. The first is justified because we only want to include the gravitational influence of the primary on the blob of matter on its way from the $L1$ point to the secondary, not the evolution of the primary itself. We restrict the primary's hydrodynamic participation to the shedding of one blob of gas from its outer layers ($m_{\rm blob} = 5 \times 10^{-4}\ M_\odot$). The secondary can be treated as a point mass because the size of the blob ($\tau_{\rm blob} \approx 8 \times 10^{11}$ cm) is large compared with the radius of the secondary ($R_2 \approx 10^{11}$ cm), which we take to be a main-sequence star. Also, the LS radius is large compared with R_2: $r_{\rm LS} \approx 0.08a \approx 14R_2$ for T CrB.

We take the speed of the blob as it leaves the $L1$ point to be the sound-speed characteristic of the envelope of the primary, and we take the blob to be in hydrostatic equilibrium until it begins to be affected by the tidal forces of the secondary. After specifying a mass $m_{\rm blob}$ and radius $r_{\rm blob}$ for the blob, we take the radial structure to be that of a polytrope with index $n = 1.5$. This fixes the central density and temperature to be $\rho_c \approx 2.8 \times 10^{-6}$ g cm^{-3} and $T_c \approx 4200$ K, respectively. This value for T_c was chosen so that the average temperature through the blob is comparable to that in the envelope of the gM3 primary (i.e., ~ 3000 K).

We adopted the polytrope model mainly for convenience. First, the correct initial distribution of density and temperature within the blob is very uncertain, because it is not clear how the giant ejects the blob. Our choice for the polytropic temperature gives the blob roughly the correct amount of internal energy per unit mass (i.e., that of the red giant's envelope); a polytropic index of $n = 1.5$ also seems reasonable for the outer atmosphere of a convective red giant. Although we assume that the blob is initially in virial equilibrium [i.e., that (kinetic energy) $= -2$(potential energy)], the evolutionary computations described below demonstrate that the blob quickly forgets the initial conditions once the blob begins to approach the accretor. Thus, the initial conditions mainly affect the preperiastron evolution, which is very uncertain anyway owing to the unknown nature of the ejection event. Our main interest is to ascertain the state of the disk at a time much longer than the local dynamical time; this result is not sensitive to the initial conditions within the blob, so we did not try additional computations with different virial coefficients or internal density laws.

Our numerical definition of the edge of the polytropic blob is the spherical shell within which the density ranges from 10^{-3} to 10^{-6} of the central density. We must smooth this shell artificially over roughly two zones to avoid an overly abrupt transition in density. Without smoothing (which has the effect of extending the edge somewhat), the transition would occur within a single zone, and the thickness of the shell would jump by a factor of 2 at an interface between a coarse and a fine grid, giving rise to problematical waves.

The equation of state used is that of a perfect gas plus radiation:

$$P = \frac{\mathscr{R}}{\mu}\rho T + \frac{a}{3}T^4 . \quad (2)$$

Effects due to nuclear burning and radiative cooling have been neglected. The first is negligible because the temperatures reached during the evolution (10^5 K) are too low for nuclear reactions to be important energy sources. Also, the timescale for cooling is much longer than the dynamical time: if the blob is optically thick, it radiates its internal energy

$$U = \frac{n}{5-n}\frac{Gm_{\rm blob}^2}{r_{\rm blob}} = \frac{3}{7}\frac{Gm_{\rm blob}^2}{r_{\rm blob}} \quad (3)$$

with a luminosity of $L = 4\pi r_{\rm blob}^2\,\sigma T^4$. Using the above values for the initial state of the blob gives an initial cooling timescale of $\tau \approx U/L \approx 1$ yr. It would be very difficult to include radiative cooling in a full three-dimensional computation such as we have. To calculate the surface emissivity, for example, one would have to calculate the frequency-dependent radiative transfer along many lines of sight traversing the system as viewed at differing orientations. Because of our neglect of cooling, we may be overestimating somewhat the degree of spreading of the blob.

2.1.1.2. Computational Procedure

Here we will only summarize the numerical techniques. They are described in detail in Ruffert & Müller (1990) and Ruffert (1992).

The distribution of matter is discretized on an equidistant Cartesian grid (zone size δ) and is evolved with the piecewise parabolic method (PPM) of Colella & Woodward (1984). For numerical reasons, both the point-mass potentials,

$$\Phi_{1,2}(i,j,k) = -G\frac{M_{1,2}}{\{d^2(i,j,k) + \epsilon^2\delta^2 \exp\left[-d^2(i,j,k)/\epsilon^2\delta^2\right]\}^{1/2}} , \quad (4)$$

and the potential of the gaseous mass,

$$\Phi_{\rm gas}(i, j, k) = -G \sum_{i'} \sum_{j'} \sum_{k'} [\![m(i', j', k') \{ r^2(i, j, k; i', j', k') + \varepsilon^2 \delta^2 \exp [-r^2(i, j, k; i', j', k')/\varepsilon^2 \delta^2] \}^{-1/2}]\!] , \quad (5)$$

were softened. The indices (i, j, k) and (i', j', k') denote cells of the grid, Φ is the potential, m is the mass in the cell, d is the distance from the point mass to the cell, r is the distance between the cells, $\epsilon = 2.5$ and $\varepsilon = 0.5$ are softening parameters, and δ is the width of one zone. We chose $\varepsilon = 0.5$ because this softening roughly imitates the smooth distribution of matter in one cubic zone. The choice $\epsilon = 2.5$ is a compromise between having very short timescales (small ϵ) and having an unrealistically extended secondary (large ϵ). The exponentials reduce the influence of the softening rapidly outside the distance given by the smoothing parameter without introducing new extrema. The following values can be obtained from algebraic manipulation for $r = 0$ (with $\bar{\epsilon} = \epsilon\delta$):

$$\Phi = \frac{1}{\bar{\epsilon}}, \quad \frac{\partial \Phi}{\partial r} = \frac{\partial^2 \Phi}{\partial r^2} = \frac{\partial^3 \Phi}{\partial r^3} = 0, \quad \text{and} \quad \frac{\partial^4 \Phi}{\partial r^4} = -\frac{6}{\bar{\epsilon}^5} . \quad (6)$$

The motion of the two point masses representing the stars is integrated by a leapfrog scheme. We neglect the gravitational force of the blob on the stars.

To follow the hydrodynamical evolution of the blob, we employ three nested grids, each with a grid spacing a factor of 2 smaller than the previous one. To resolve better the flow at small radii in the protodisk, we fix the center of the multiply nested grids on the position of the accreting secondary. This positioning scheme is different from that described in Ruffert (1992), wherein the coarsest grid is centered on the center of mass of the system.

2.1.1.3. Initial Conditions

To begin the calculation, we fix the number and structure of objects to be modeled as well as their positions and velocities. We have already described most of these parameters above: the primary and secondary orbit each other on circular orbits as point masses. We idealize the blob to be a polytropic sphere which is launched from $L1$ toward the secondary with a velocity of the thermal speed characteristic of the gas in the envelope of the gM3 star (i.e., $\sim 5 \times 10^5$ cm s^{-1}). It is not expedient, however, to start the full hydrodynamical calculation from that point in time: (1) the tidal forces act effectively only when the distance from the blob to the secondary is approximately the diameter of the blob, and (2) the resolution of the blob decreases with increasing distance from the secondary (it is discretized only on the coarsest grid at this distance).

As a first approximation of the orbit during this prehydrodynamic stage, we model the motion of the blob as a point mass moving under the influence of the two stars. After approximately 30 days the blob is near enough to the center of the grids ($\approx 2.8 \times 10^{12}$ cm) to be adequately resolved on the second finest grid (i.e., the middle one of the three). We then take the positions and velocities of the three objects from this three-body calculation and plug them into the full hydrodynamical model.

Table 1 summarizes important parameters for the models that we calculated and includes some results.

2.1.2. *Results*

2.1.2.1. Orbits

Figure 1 compares the orbit of the blob's center of mass taken from the hydrodynamic computations with the orbit of a point mass in the same potential. The three curves shown for the point mass represent trajectories with different initial velocities. The resulting orbits (P1–P3) differ only slightly. This is due to the fact that the initial velocities (which are all within a factor of 2 of the gM3 envelope sound speed) are more than 10 times smaller than the velocities reached at periastron.

As long as the deformation of the blob due to tidal forces is small, the orbit of the blob (B1 and B2 in Fig. 1) will coincide with the orbits of a point mass. Shortly before periastron (at about 33 days) the deformation becomes important, so that the point at which apastron is reached (at about 45 days) is shifted clockwise and moved to smaller radii with respect to the point-mass apastra. This behavior shows that orbital energy (kinetic and potential) has been transferred to internal energy in the hydrodynamic calculations as one would expect from the nature of the tidal force. Also, B1 and B2 differ (after approximately 35 days) because the three-zone wide edge of the blob (see § 2.1.1.1) interacts with the secondary during periastron. This interaction is reduced for model H64, which has the higher resolution (i.e., B2).

TABLE 1

INITIAL CONDITIONS AND RESULTS OF MULTIPLE GRID MODELS

Model	N	L (10^{12} cm)	δ (10^{10} cm)	m_l (%)	t_f (days)
H32.....	32	16	12.5	10	75
H64.....	64	16	6.25	4	75

NOTE.—N is the number of zones per dimension, L is the size of the largest grid, $\delta = L/N$ is the size of one zone on the finest grid, m_l is the fraction of mass lost from the grid at t_f, t_f is the total time of the run (note that the hydrodynamic model only begins at 29.6 days).

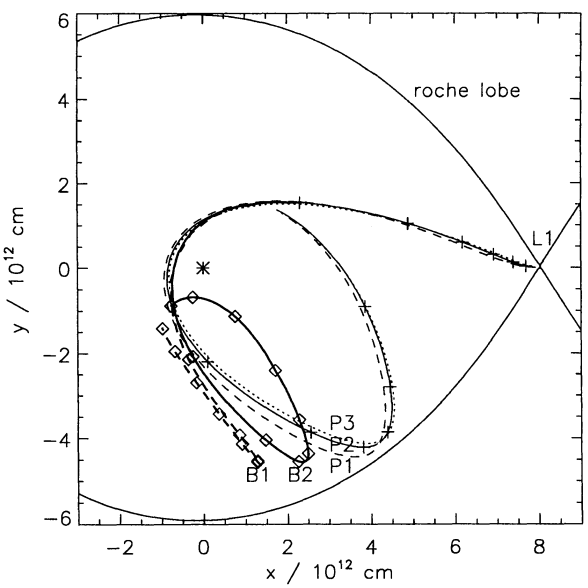

FIG. 1.—Thin lines show the orbits of a point mass (P1–P3) in the potential of a binary in the corotating frame of reference. The secondary is at $x = 0$, the primary at $x = 1.7 \times 10^{13}$ cm, and the Lagrangian point $L1$ at $x = 0.8 \times 10^{13}$ cm. (For all three $y = 0$.) The blob started at $L1$ with a velocity in the direction of the secondary of 0.5 (P1), 1.0 (P2), and 2.0 (P3) times the sound speed (5×10^5 cm s^{-1}). The orbits differ only slightly during the first 60 days (the tick marks show intervals of 5 days). The heavy lines show the orbit of the center of mass of the gas on the grid for the two hydrodynamic models: B1 for H32 (*dashed line*) and B2 for H64 (*solid line*). At first the orbits B1 and B2 closely follow the orbit of a point mass (P1–P3), but as tidal forces begin to act they deviate more and more from each other.

As an aside we mention here that Webbink (1976) and WLTO note a dip in the visual light curve of T CrB which occurred about 260 days before the primary maximum, and interpret it as being evidence for the ejection of the blob. Thus 260 days should be approximately the diffusion time for the blob to spread over its entire orbit about the secondary (see also the footnote on p. 657 of WLTO). Combining our three-body experiments in which the blob is ejected at roughly the sound speed of gas in the gM3 envelope star with the three-dimensional hydrodynamical results indicates, however, that this time would only be about 63 days. Thus it appears that either (1) the local minimum in the light curve pointed out by Webbink (1976) and WLTO was unrelated to the blob ejection or (2) there is some systematic effect which obviates this direct comparison. Given the complexity of the real system, it may be that a factor of ~ 4 disagreement in this timescale is not serious.

2.1.2.2. Density Distribution and Dynamics of the Flow

Figures 2–4 show snapshots of the density distribution and velocity flow in the orbital plane for model H64. The secondary (accretor) is always placed at the origin of the panels. In this frame of reference the primary starts out at ($x = -17 \times 10^{12}$ cm, $y = 0$) and rotates counterclockwise. It passes ($x = 0$, $y = -17 \times 10^{12}$ cm) after a quarter of an orbital period, i.e., ≈ 57 days. The position of the primary is given in the figure legends.

Figures 2*a* and 2*b* show the initial setup for the hydrodynamic calculation ($t = 29.6$ days). The polytropic structure quickly gets deformed by tidal interaction as the blob approaches the accretor (Figs. 2*c* and 2*d*). At periastron ($t = 33.2$ days, Figs. 2*e* and 2*f*) the blob is banana-shaped: its length-to-width ratio is about 4, and it is bent by about 45°. This somewhat torus-like shape is not maintained for long, however. The matter still has enough kinetic energy to move out of periastron on an orbit with high ellipticity.

The tidally deformed blob expands further as it recedes from the accretor (Figs. 3*a* and 3*c*). Matter that stays near the accretor continues to stretch the leading edge of the blob by winding it up around the accretor: A mushroom-shaped distribution forms (Fig. 3*b*). After apastron (around $t = 48$ days, shown in Figs. 3*c* and 3*d*), the bulk of the blob approaches the accretor a second time. It is stretched and bent further, nearly forming a semicircle (Figs. 3*e* and 3*f*). Again, this distribution is only short-lived: differential velocities spread the material into a more axisymmetric, disklike shape. The density and velocity distribution at the end of the calculation is shown in Figures 4*a* and 4*b*. The Roche volume of the accreting star becomes almost completely filled (albeit not at a uniform density). Figure 5 shows the temperature distribution in the orbital plane at the end of the run. The temperature ranges from $\sim 10^4$ K near the inner edge to $\sim 10^5$ K near the outer edge. After the protodisk has formed, the material is sufficiently spread out that cooling should become more important than it was during the early stages when the blob was compact and roughly spherical. During the observed ~ 100 day interval between maxima in T CrB this matter would probably cool to a few thousand degrees.

The degree of conservation of various global physical quantities can be examined in Ruffert (1992), which used the same PPM method as the one underlying our calculations. The constancy of the global angular momentum, for example, is dependent on what fraction of the mass remains on the grid. If no mass is lost, angular momentum is conserved to within about 2%. (The method is exactly conservative only in mass, linear momentum, and energy.)

In our application, the blob initially has a uniform velocity, so it does not have any rotation about its center of mass (hence no net angular momentum). As it becomes distorted, it acquires angular momentum. Since there are no obvious strong shocks which might induce a net vorticity, it would appear that the tidally elongated blob interacts with the binary and gets rotated by "external" torques (the torques are internal to the binary but external to the gas). Were our numerical finding of the lack of any strong shocks to be taken literally, it would argue against the production of the primary maximum via blob circularization. The torque-induced spin-up is to be expected, and has been seen in previous computations which investigated the tidal disruption of a gas blob by a massive central object (see, e.g., Evans & Kochanek 1989). Because of this effect, there might appear to be a discrepancy between the estimate of the specific angular momentum radius (the "Lubow-Shu radius") cited by CK, and the typical radius of the matter in the postperiastron distribution seen in the previous figures. (Actually there was an error in CK, which has been corrected below in footnote 3.) The estimate of CK was taken from Lubow & Shu (1975; see also Hut & Paczyński 1984) and is based on an irrotational stream which leaves the $L1$ point and falls toward the accreting star without acquiring any vorticity. There is no account taken of a tidally induced torque, since the individual fluid elements comprising the stream do not act coherently as an extended mass that is capable of being torqued. Therefore, the CK estimate is not directly applicable to the PPM calculations.

2.1.2.3. Averaged Density Distributions

To be able to compare with more traditional one-dimensional and two-dimensional calculations of disks, we now present some averaged density distributions. Figure 6 shows the surface density projected onto the (x, y) orbital plane near the end of model sequence H64, and Figure 7 shows the same density distribution averaged azimuthally about an axis perpendicular to the orbital plane which goes through the accretor. One notices only a slight dependence of the relatively flat surface density distribution on the azimuth in Figure 6, whereas the azimuthal average of density (Fig. 7) reveals a disklike structure. The aspect ratio h/r for the bulk of the matter in Figure 7 is about 0.2.

As a second step, one can merge the information presented in Figures 6 and 7 to obtain the azimuthally averaged surface density in the radial direction projected onto the orbital plane. This is shown in Figure 8. The matter distribution becomes fairly flat after roughly a dynamical timescale. Although a torus-like object seems to have formed with a density contrast of about 5, it is only transient. The subsequent thermal expansion tends to fill the central regions. Artificial (i.e., numerical) viscosity may be at least partly responsible for the spreading of the torus. One expects from the energetics that, to overcome the centrifugal barrier, the internal energy per unit mass must be comparable to the potential energy difference spanning the radii over which spreading occurs. This is equivalent to saying that the gas temperature in the torus has to be of the order of the virial temperature, i.e., $T \sim GM_2 m_p/(kr) \simeq 3 \times 10^6$ K $(M_2/1.6\ M_\odot)/(r/10^{12}$ cm). The temperatures seen in Figure 5 are much smaller than this, showing that numerical viscosity plays a role in the spreading.

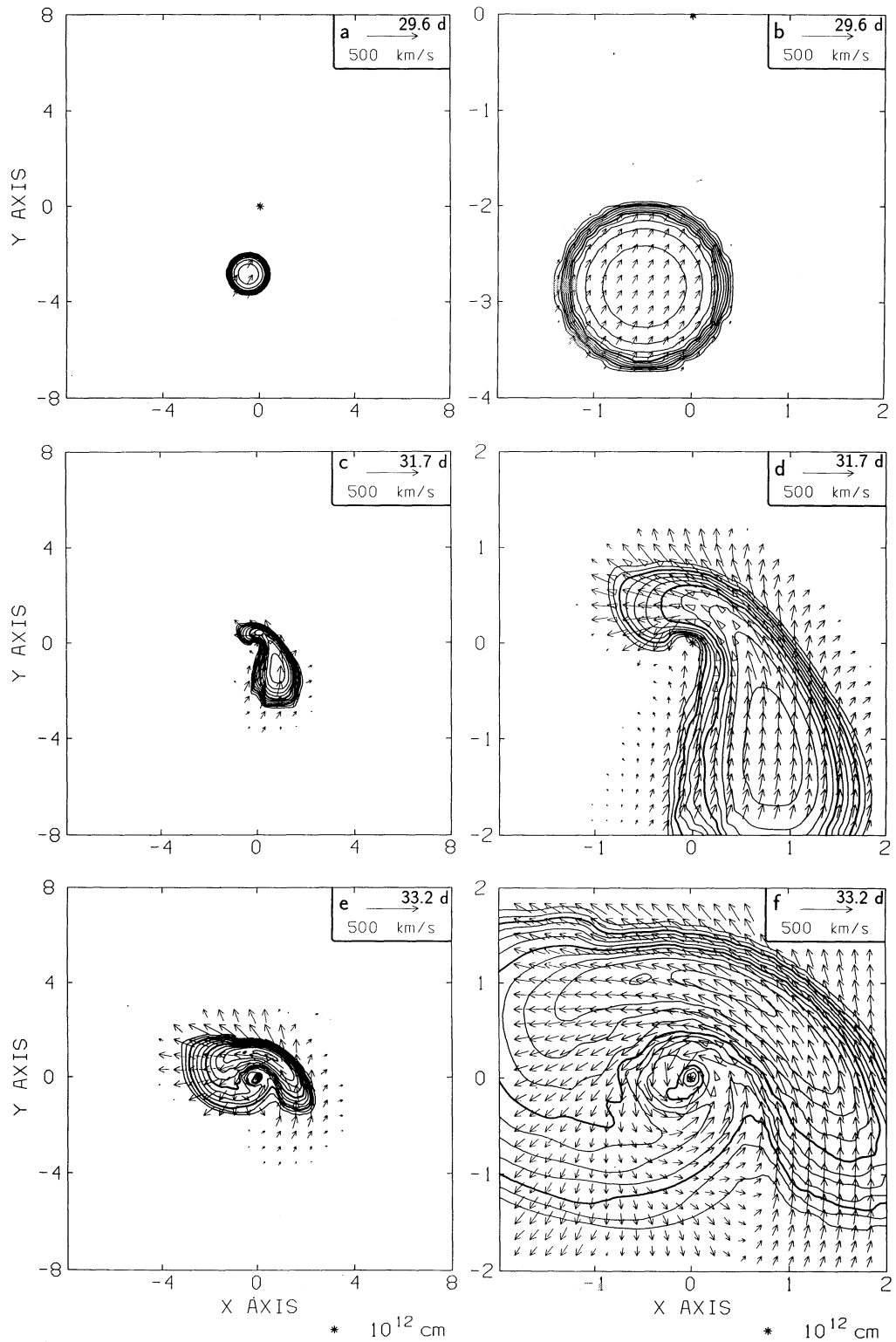

FIG. 2.—Contour plots showing snapshots of the density together with the flow pattern in the orbital plane for model H64 at different times. The contour lines are logarithmically spaced with intervals of 0.5 dex. The two bold contours correspond to $\rho = 10^{-10}$ and $\rho = 10^{-8}$ g cm^{-3}. The position of the secondary (accretor) is marked by an asterisk. The inset in each panel gives the scale for the velocity and the time elapsed in days. The right-hand panels (*b*, *d*, *f*) enlarge the area around the secondary fourfold relative to the left-hand panels. The position of the primary in units of 10^{12} cm is (−11.4, −12.3) for panels *a* and *b*, (−10.6, −13.0) for panels *c* and *d*, and (−10.0, −13.4) for panels *e* and *f*, respectively.

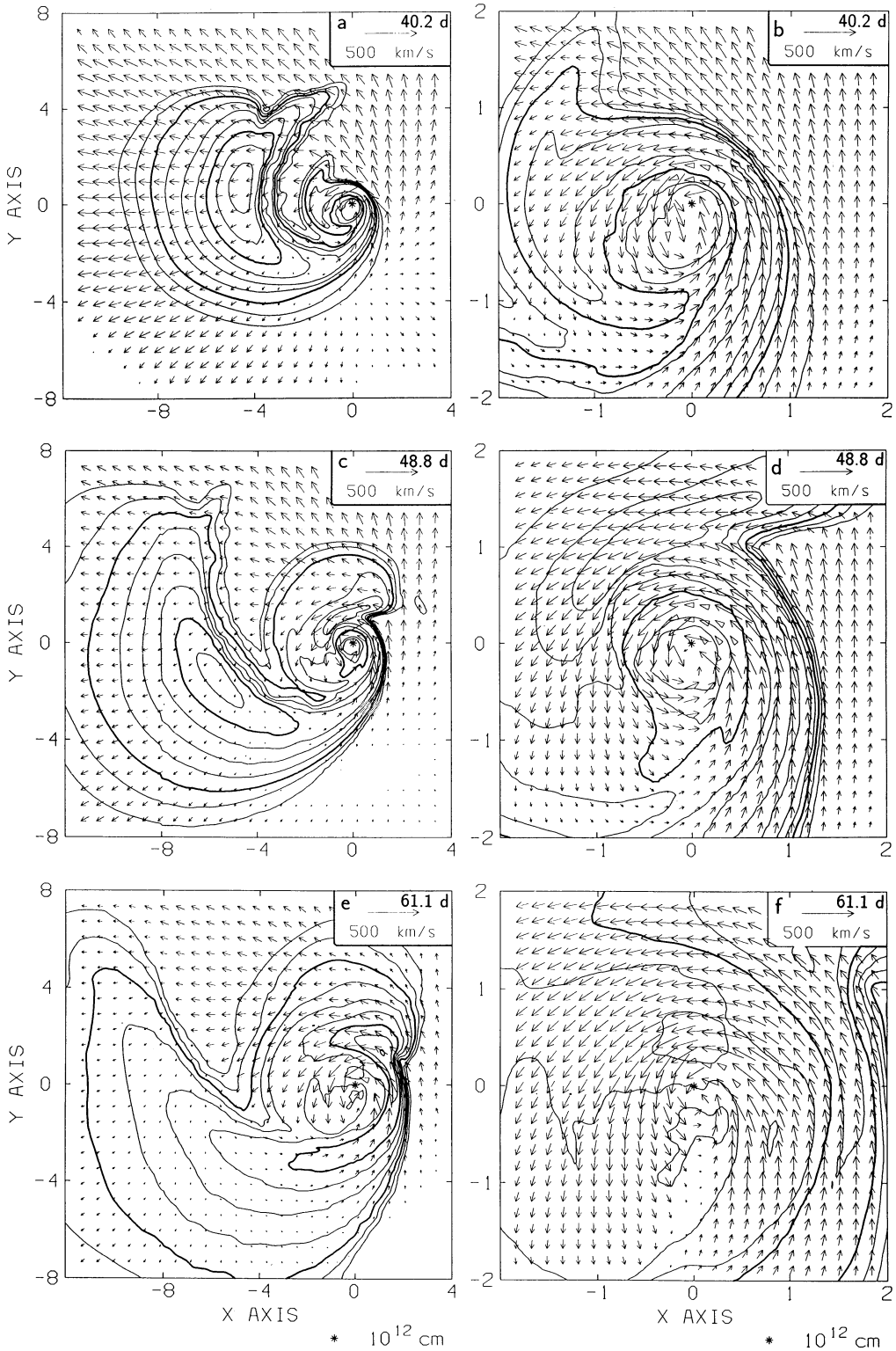

FIG. 3.—Contour plots showing snapshots of the density together with the flow pattern in the orbital plane for model H64 at different times (continuing from Fig. 2). The description of the panels can be found in the legend of Fig. 2. The position of the primary is (−7.3, −15.1) for panels *a* and *b*, (−3.5, −16.4) for panels *c* and *d* and (+2.3, −16.7) for panels *e* and *f* (all in 10^{12} cm), respectively.

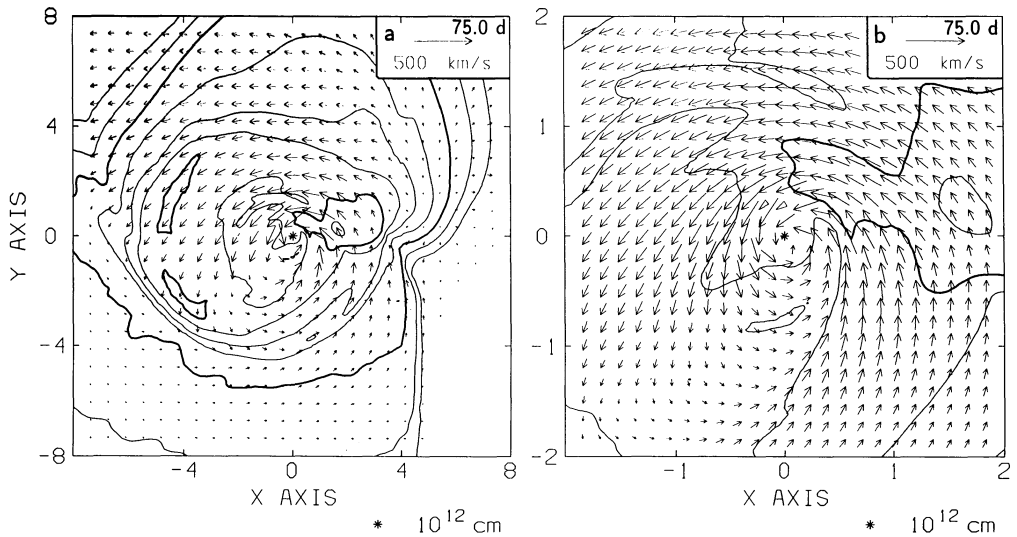

FIG. 4.—Contour plots showing snapshots of the density toegether with the flow pattern in the orbital plane for model H64 at the end of the run (continuing from Figs. 2 and 3). The description of the panels can be found in the caption of Fig. 2. The position of the primary is (+8.3, −14.7) for panels *a* and *b* (all in 10^{12} cm).

Figure 9 shows (1) the maximum density over the entire grid and (2) the density at the position of the accreting star. There is about a factor of 10 difference between the two. Initially (i.e., at $t \approx 32$ days) high-density material is flowing by the secondary (accretor). The high specific angular momentum then sweeps the immediate vicinity of the accretor free of matter, causing the density to drop drastically. It rises again slowly while the (now) very distended blob approaches the secondary a second time. The smooth decline of the top curves is due to the expansion of the blob. At about 53 days the position of the maximum density shifts from the center of the expanding blob to nearer the accretor, where matter has had the time to collect. The variations of the curves belonging to the H32 model are less pronounced than those of the H64 model because lower resolution leads to smaller gradients.

Despite performing the computations on a Cray YMP, we are limited by CPU time and are able to follow the evolution of the blob for only about 45 days (cf. Table 1). This only takes us up to about 12 days after periastron. Near periastron the tidal force is most effective at heating the blob matter; we therefore anticipate that the observed primary maximum in the light curve of T CrB would correspond roughly to this point in the computations. Thus our final state shown in Figures 7–9 represents the configuration at about 85–95 days before the observed secondary maximum. Given the amount of smearing that has already occurred during our computations, we fully expect that another ~90 days of evolution would lead to a very nearly axisymmetric system with essentially constant surface density (when projected onto the orbital plane). Thus,

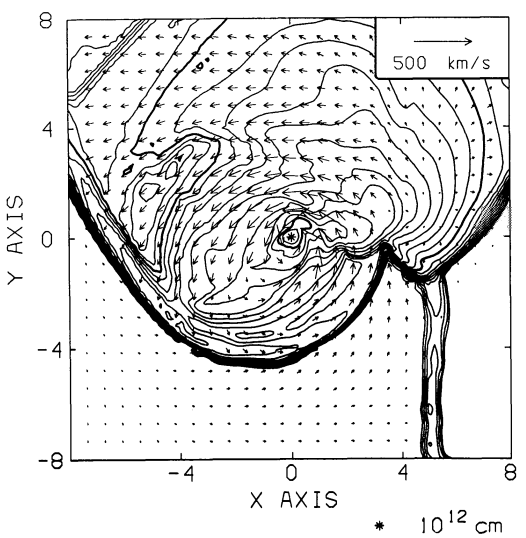

FIG. 5.—Contour plot of the temperature accompanying Fig. 4*a* together with the flow pattern. The contour lines are logarithmically spaced with intervals of 0.1 dex. The two bold contours correspond to $T = 10^4$ K and $T = 10^5$ K.

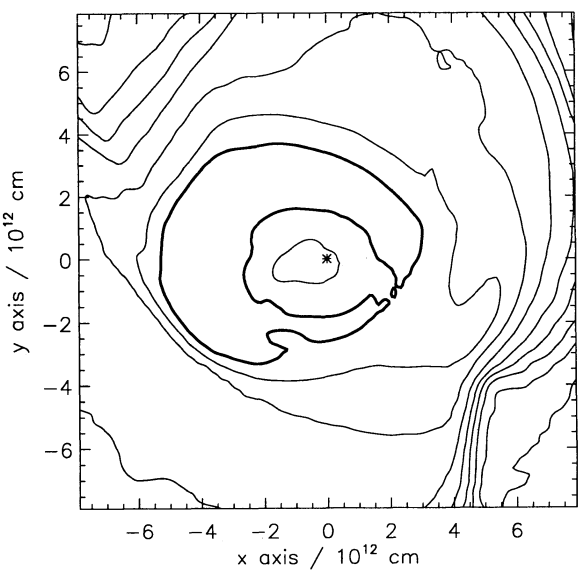

FIG. 6.—Surface density distribution of model H64 at $t = 70$ days obtained by projection onto the orbital plane. The contours are logarithmically spaced with intervals of 0.5 dex. The bold contour represents $10^{4.5}$ g cm^{-2}. The asterisk denotes the position of the secondary (accretor).

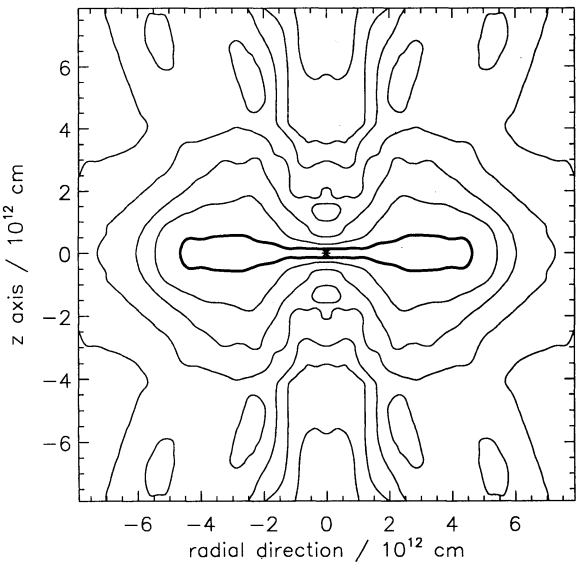

FIG. 7.—Azimuthally averaged density distribution around a line perpendicular to the orbital plane extending through the accretor. The profile is for model H64 at $t = 70$ days. The contours are logarithmically spaced with intervals of 0.5 dex. The bold contour represents $10^{-8.5}$ g cm^{-3}. The asterisk denotes the position of the secondary (accretor).

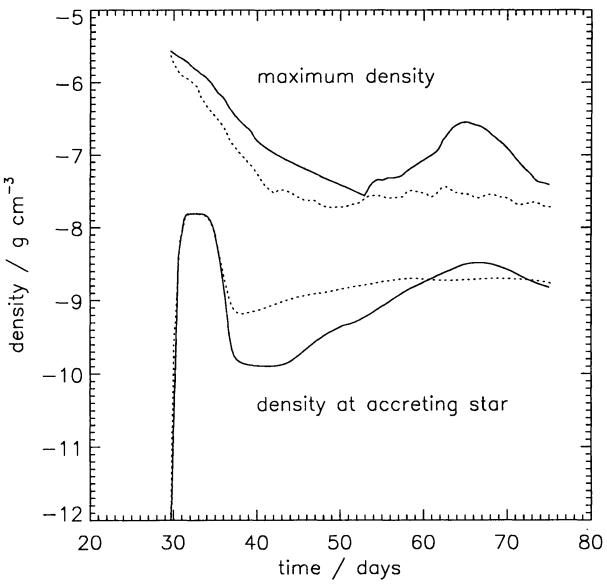

FIG. 9.—Maximum density over the grid and density at the accreting star as a function of time. The dotted lines show the model H32, and the solid lines are for H64.

even if we overestimate the rate of smearing by neglecting cooling of the spreading blob, we are confident that, given the amount of time the system has to evolve, the final state will have a flat surface density distribution as we have envisioned.

2.1.2.4. Global Values

During its evolution the blob becomes very distended and fills the Roche lobe of the accreting star. Only a small amount of matter becomes unbound from the system and flows off the coarsest grid, however. In the higher resolution model H64 only approximately 4% is unbound at the end of the calculation (at $t = 75$ days). So most of the matter will collect in the protodisk forming around the accretor.

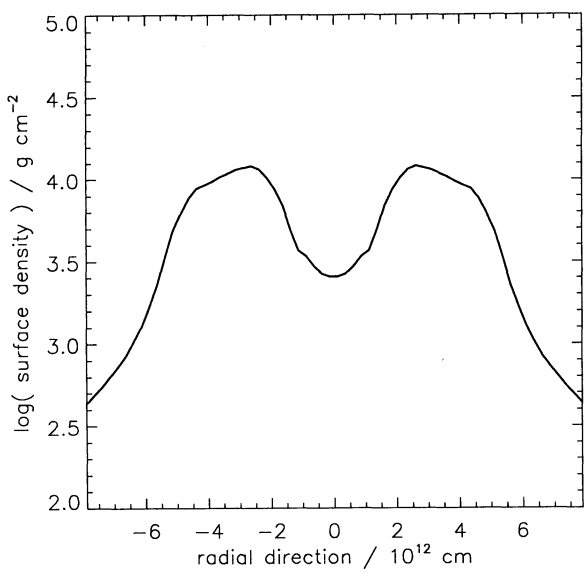

FIG. 8.—Surface density as a function of radial direction

2.2. *One-dimensional Simulations of the Accretion Disk*

The computations presented in the previous section show that the starting conditions used by CK in their modeling of the secondary maximum in the 1946 outburst for T CrB are unlikely to be realistic. It now appears improbable that a well-defined torus of matter would be able to survive for ~ 100 days after the primary maximum (when the centroid of the blob was near periastron of the mass gainer). One hundred days is ~ 15 orbital timescales at the LS radius. In much less than 100 days the blob would have become so spread out that it would form a uniform disk having roughly constant surface density within the Roche lobe of the mass-gaining star. Furthermore, one cannot isolate as separate physical effects the spreading of the blob in the directions parallel and perpendicular to the velocity vector of the blob: CK envisioned the blob being stretched out along the direction of the orbit by tidal forces alone until the leading edge merged with the trailing edge, so that eventually the gaseous matter would have roughly the configuration of a slightly eccentric torus. From the three-dimensional PPM results we see that this is unphysical. Disruption from tidal forces and spreading due to internal gas pressure of the blob occur simultaneously. The blob would have to be extremely cold to be pointlike enough to avoid smearing in the perpendicular direction, but this would also prevent smearing in the parallel direction. Also, even if the blob managed to remain somewhat intact after one periastron passage, subsequent passes near the MS star would disrupt it and cause significant spreading through tidal interactions alone. It is therefore reasonable to reexamine the results of CK within the context of a model in which the starting condition is a disk with surface density $\Sigma(r)$ constant rather than a Gaussian profile peaked at r_{LS}. In addition, CK had as a further free parameter the fraction of the blob which remains bound to the mass gainer. From the previous section we get the result that this fraction is roughly unity; therefore, since Webbink postulated a blob of $5 \times 10^{-4}\ M_{\odot}$, we also take this to be our standard starting value.

CK found that, because the observed rise time of the secondary maximum was short compared with the ~100 day interval between primary and secondary maxima, it was necessary to have the accretion disk viscosity parameter α remain quite small initially and then increase rapidly after ~100 days. On physical grounds one expects the Keplerian shear to drive the viscous dissipation in the accretion disk; therefore, if one establishes an accretion disk very quickly with a small seed viscosity, one would expect α to grow as

$$\alpha(t) = \frac{\alpha_f}{1 + (\alpha_f/\alpha_i)e^{-t/\tau}} .$$

CK's assumption of an initially Gaussian $\Sigma(r)$ profile centered at r_{LS} for the torus[3] led them to adopt a constant value $\tau = t_{orbit}(r_{LS})$. Since most of the mass is concentrated near r_{LS} in this picture, it was reasonable to take one growth rate for $\alpha(t)$ over the entire disk. In our revised picture the starting point is a configuration of matter with $\Sigma(r)$ = constant, and therefore we must take into account the range in growth times over the radial extent of the disk. In addition, we now take $\tau \sim 1/\Omega(r)$ instead of $2\pi/\Omega$ as was done by CK. The physical motivation for this is the large growth rates found in the numerical study of Hawley & Balbus (1991). Although we do not necessarily advocate their specific instability, it is worth noting that the fastest-growing modes of an instability which couples very strongly to the shear appear to have growth times of roughly $1/\Omega$ rather than $2\pi/\Omega$. Therefore, for generality we adopt the faster timescale on the expectation that the mechanism with the most rapid growth rate will dominate, and that this rate will be $\sim\Omega$. Since Ω varies as $r^{-3/2}$ in Keplerian disks, the inner regions reach saturation much sooner than the outer regions. In addition, since the growth times are now faster than in CK, we must reduce α_i: in our current models $\alpha_i \sim 10^{-6}$ to 10^{-5}.

We use the same accretion disk computer code as in CK (which is described in Cannizzo, Lee, & Goodman 1990 and based on that of Bath & Pringle 1981). We use the collection of tabular opacities described by Cannizzo (1992) rather than the analytical fits employed by CK. Figure 10 shows our model light curves for the secondary maximum in T CrB for runs starting with a flat surface density profile. The two sets of curves show models in which the growth time for $\alpha(t)$ is $1/\Omega$ and $2/\Omega$. For comparison we also show one of the light curves computed by CK. The two most noteworthy differences between the old computations and the new ones are that there is (1) significant accretion luminosity during the time preceding the secondary maximum (an artifact of the nonnegligible surface densities at small radii initially) and (2) a faster rise time within ~1–2 mag of the peak. The latter effect is due to the smaller adopted growth times which ensure that many more e-folding times will be contained within the ~100 day interval between $t = 0$ and the peak in the secondary maximum.

Figure 11 shows the evolution of $\alpha(r, t)$ for times which are multiples of 10 days after $t = 0$. Since α increases first at small radii, the inner parts of the disk will evolve faster and accrete onto the MS star sooner than the outer regions. Also, since there is now accretion almost immediately after $t = 0$ (the time of primary maximum), there is a significant contribution to the luminosity of the system long before the start of the secondary maximum.

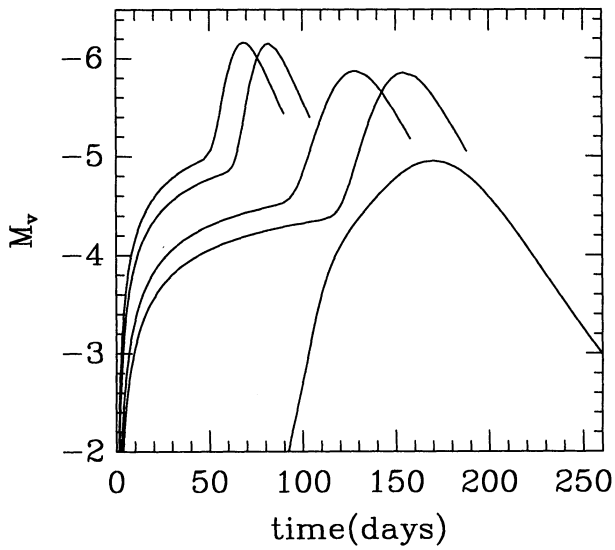

FIG. 10.—Absolute magnitude for a face-on disk vs. time. We assume blackbody flux distributions corresponding to the effective temperature in each annulus. Going from left to right, the five curves show the evolution for (1) $\tau = 1/\Omega$, $\alpha_i = 10^{-5}$; (2) $\tau = 1/\Omega$, $\alpha_i = 10^{-6}$; (3) $\tau = 2/\Omega$, $\alpha_i = 10^{-5}$; (4) $\tau = 2/\Omega$, $\alpha_i = 10^{-6}$; and (5) the run shown in the top panel of Fig. 3 of CK. Here τ is the local growth rate for $\alpha(t)$ and α_i is the initial "seed" viscosity. For all runs we take an initial disk mass of $5 \times 10^{-4}\ M_\odot$ and a saturation viscosity $\alpha_f = 3$. For the first four runs the initial density is constant with radius, whereas for run 5 it is the Gaussian profile described in CK.

Figure 12 shows the evolution of the surface density, again at 10 day intervals. Because the inner regions have a much higher viscosity initially than the outer regions, there is a strong tendency for the high-α matter to spread outward. Consequently, one sees an outward-spreading wave which travels at the interface of the high/low-α regions. In Figure 13 we show the evolution of the vertically averaged temperature. Figure 14 shows

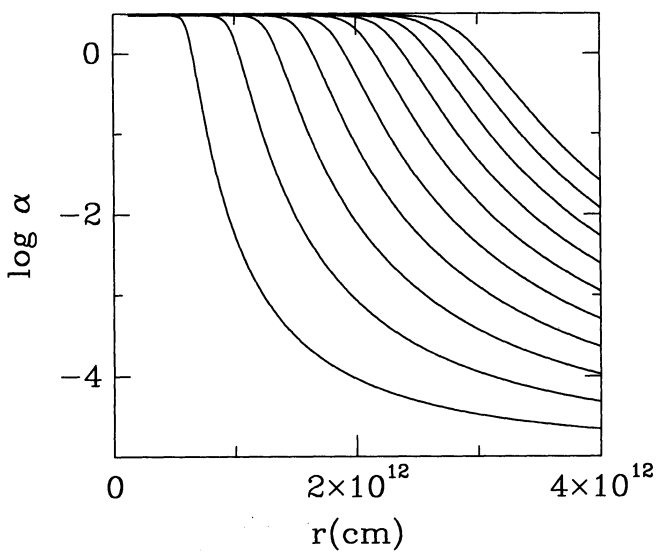

FIG. 11.—Variation of α with radius and time. This evolution is for run 3 in Fig. 10, our "standard model." The curves correspond to t(days) = 10, 20, ..., 100. Since the growth rates are faster for smaller radii, these regions reach saturation sooner than portions of the disk lying at larger radii.

[3] CK erroneously took for the Lubow-Shu radius $r_{LS} = 2 \times 10^{12}$ cm, which gives an orbital time of 22.6 days. Both LS and Hut & Paczyński (1984) show that for our mass ratio $q \sim 0.75$ we should have $r_{LS}/a = 0.078$, giving $r_{LS} = 1.32 \times 10^{12}$ cm and $t_{orbit} = 7.57$ days. Since both r_{LS} and t_{orbit} should have been smaller, the value of $\alpha_i = 0.001$ used by CK would be relatively unchanged.

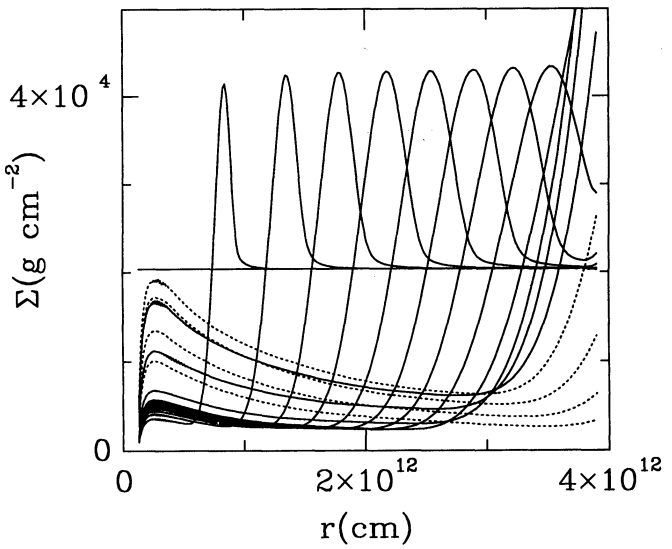

FIG. 12.—Variation of the surface density Σ in the standard model for t(days) = 0, 10, 20, ..., 160. The "α-wave" caused by the spread of the high-viscosity material at small radii is accompanied by a spike in Σ. As the wave passes a given radial location, the matter interior to that point merges into the quasi-steady disk. The four dashed curves indicate times after maximum brightness (i.e., $t \geq 130$ days).

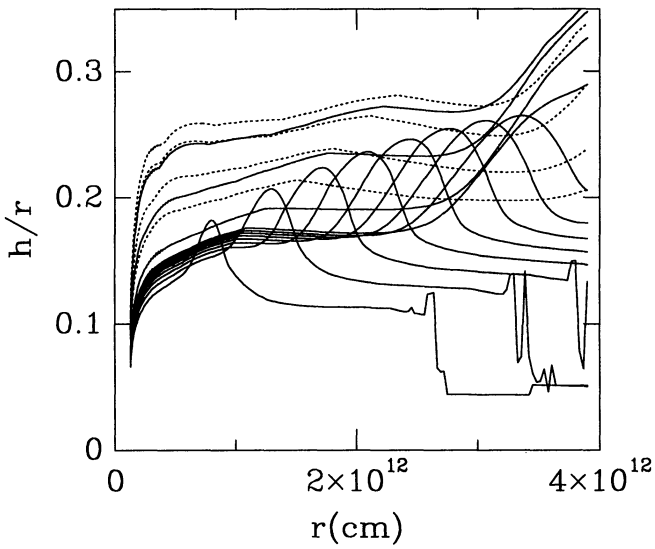

FIG. 14.—Variation of the disk semithickness h in the standard model for t(days) = 10, 20, ..., 160 days.

the corresponding evolution of the disk semithickness h. Note that h is in general a few tenths, which is in rough accord with the end state of the PPM computations (e.g., Fig. 7). By examining Figures 12–14, we see that there are in fact two outward-moving transitions: (1) the one between high- and low-α regions which can be identified by the spikes in Σ and T, and (2) a separation between ionized and neutral material revealed by the abrupt change in temperature at $T \approx 10^4$ K. The ionized inner regions lie on the upper stable portion of the "S-curve" (e.g., Cannizzo & Wheeler 1984), whereas the neutral outer regions reside on the lower stable branch of the S-curve. From Figure 11 we infer that the high/low-α transition occurs at $\alpha \approx 10^{-1.5}$, whereas the ionized/neutral transition occurs at $\alpha \approx 10^{-4.0}$. Thus we have a picture in which two concentric transition waves propagate outward. They travel at the same speed ($\sim 4 \times 10^5$ cm s^{-1} from Fig. 12), since the same physical effect is responsible for producing both of them, namely, the wave of increasing α. In dwarf novae the transition between the two temperature states characterizing quiescence and outburst is triggered when the surface density in the accretion disk becomes equal to one of the critical surface densities corresponding to local extrema in the S-curve. This is also true in the present computations; however, the critical surface densities are continuously changing as $\alpha(r, t)$ evolves. Thus our "heating front" comes about solely because the regions of the disk lying at smaller radii have a faster growth rate for α to increase, and therefore the critical surface densities drop below the actual surface density $\Sigma(r)$ first in the inner regions. The interface at which $\Sigma(r) \approx \Sigma_{\rm crit}$ moves outward with time. To be fully consistent, however, we should solve not only the viscous diffusion equation for $\Sigma(r, t)$ but also a thermal equation for $T(r, t)$ as is done for dwarf novae. This would give for the second transition an accompanying spike in Σ (narrower than the Σ spike for the first transition), and, more important, the speed of the heating front would then not necessarily be the same as that of the α-wave. Meyer (1984) estimates $v_F \approx \alpha\Omega h$ for the heating front speed. Using $\alpha \approx 10^{-4.0}$, $M_{\rm acc} = 1.6\, M_\odot$, $h/r \sim 0.2$, and taking a representative $r = 10^{12}$ cm, gives $v_F \approx 200$ cm s^{-1}, much slower than the α-wave speed cited above. One can imagine, however, that the system would be self-regulating in that the front speed v_F would tend to become equal to the α-wave speed v_α in the following way: as the α-wave began to catch up to the slower heating transition wave, α at the ionized/neutral interface would increase. Since v_F scales with α, the heating front speed would rise accordingly. Conversely, if v_F began to exceed v_α, the ionized/neutral transition would move away from the α-wave into lower α regions and slow down. There is another factor besides the difference in front speeds which tends to make the heating front lie at smaller radii: our disk evolution code is based on vertically

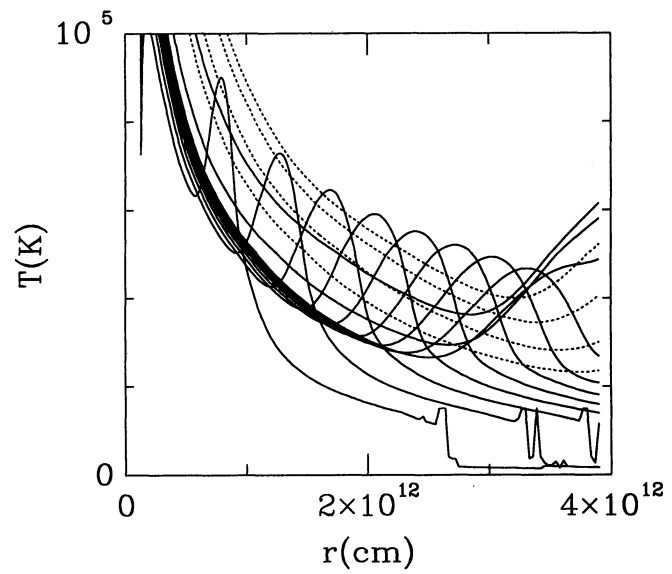

FIG. 13.—Variation of the vertically averaged temperature T in the standard model for t(days) = 10, 20, ..., 160. We see the two distinct transitions, one associated with the α-wave (indicated by the spike in T) and one associated with the interface between ionized and neutral matter (indicated by the sudden drop in T below 10^4 K). For the two reasons discussed in the text we anticipate that the latter transition would actually occur nearly coincident with the first.

averaged quantities, and Cannizzo & Reiff (1992) noted that this prescription underestimates the surface densities associated with the local extrema in the S-curve by about a factor of 10 because of the neglect of convection. From vertically explicit computations of the accretion disk structure, the critical surface densities are roughly 10 g cm^{-2} $\alpha^{-0.8}$ $(r/10^{10}$ cm$)$ $(M_{acc}/M_{\odot})^{-1/3}$ (e.g., Cannizzo, Shafter, & Wheeler 1988), which for $\alpha \approx 10^{-4.0}$ and $r \approx 10^{12}$ cm gives $\Sigma_{crit} \sim 10^5$ g cm^{-2}. Yet from Figure 12 the values of Σ_{crit} must lie at $\sim 10^4$ g cm^{-2} in our computations, since this is the initial surface density of the disk. This value is too small by roughly the expected factor of 10. Therefore, the transition should actually be occurring in accretion disk material lying at higher α-values, or equivalently, smaller radii. Our expectation, therefore, is that a more sophisticated computation which included (1) departures from thermal equilibrium and (2) scalings of $T(\alpha, \Sigma)$ determined from complete vertical structure computations would show the α-wave and heating front transitions to be roughly coincident. This would have the effect of reducing slightly the disk luminosity for early times compared with what we show in Figure 10, since the hot region would be smaller. This is not a big effect, however. We tried computing the disk brightness by summing only over radii lying interior to the α-wave. The results were only slightly different from those shown in Figure 10. In a fully self-consistent computation this may not be true.

Figure 15 shows the rate of mass flow through a cylinder of radius r as a function of time. Values of $\dot{M}(r) > 0$ indicate outflow, and $\dot{M}(r) < 0$ indicates inflow. The α-wave is revealed by the outward-moving spike in $\dot{M}(r)$. After this wave has passed a given radial location, $\dot{M}(r)$ becomes negative as the matter merges onto the quasi-steady disk which forms inside the transition annulus between low- and high-α material. Note that our outer boundary condition of a "brick wall" where $v_r \rightarrow 0$ is evident in Figure 15 as the point where $\dot{M}(r) \rightarrow 0$ for $r \rightarrow r_{outer}$. The maxima in the light curves shown in Figure 10 correspond to the times when the heating front has reached the outer disk edge and the bulk of matter in the disk begins to flow inward. The accretion rate $|\dot{M}(r)|$ is largest for the $t = 120$ day curve. For $t > 120$ days $|\dot{M}(r)|$ steadily decreases with time at all radii as matter accretes onto the MS secondary. Furthermore, since there is no mass input from the outer edge to replenish the disk, $|\dot{M}|$ is a decreasing function of radius for these later times.

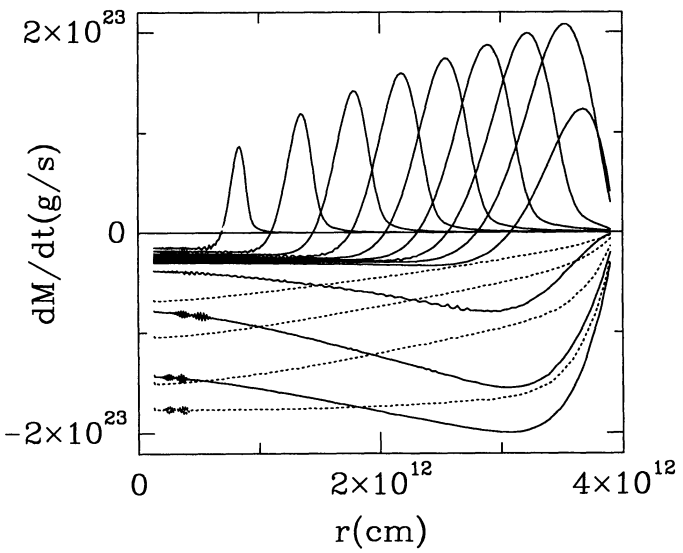

FIG. 15.—Variation of the local mass flow in the standard model. Positive values indicate outflow, and negative values inflow. The times are again multiples of 10 days, and the dashed curves correspond to $t > 120$ days. At $t = 0$ the viscosity is very small at all radii, and $\dot{M}(r) \approx 0$ everywhere. As α begins to increase in the inner regions, $\dot{M}$ becomes negative there and accretion onto the central star begins. Slightly farther out the high-viscosity matter expands into the very low viscosity disk. As more of the disk reaches the saturation viscosity α_f, the mass inflow becomes greater. The flow rate peaks near $t = 120$ days, when the bulk of the matter which lies at the outer edge of the disk finally attains $\alpha \approx \alpha_f$. This sudden addition of matter to the inflowing region causes the local maxima in the light curves for runs 1–4 seen in Fig. 10. For later times $\dot{M}(r)$ is everywhere negative, as all the disk matter gradually accretes onto the MS star.

3. DISCUSSION

We have continued a line of inquiry begun by CK into the implications of the model by Webbink (1976) which attempts to account for the 1946 eruptive behavior of T CrB. CK assumed as a starting point in their computations a narrow torus of disk matter with a Gaussian profile in $\Sigma(r)$ and a FWHM of $r_{torus}/10$. The torus radius was taken to be the Lubow-Shu radius. This configuration for the predisk state was their idealization of the postcircularization blob left over in the Webbink model after the production of the primary maximum. CK experimented by varying the FWHM by factors of a few and found no substantial differences in the ensuing light curves. An essential aspect of their model was a significant drop in Σ between the accreting star and r_{LS}. Now we have presented three-dimensional simulations which take into account spreading from internal gas pressure within the blob of matter and tidal disruption by the accreting star. The initially spherical blob is disrupted in a dynamical timescale. The distribution of matter which made up the blob becomes extremely smeared out on a timescale short compared with the observed ~ 100 day time interval between primary and secondary maxima—to the point of having a roughly flat Σ distribution within the Roche lobe of the accreting star. Our three-dimensional computations also show that nearly all the blob material remains within the potential well of the secondary. Other hydrodynamical simulations of mass flow in interacting binary systems have typically dealt with situations in which the mass transferred into the disk over an orbital time is small compared with the mass already present in the disk. This leads to a natural tendency for material to accumulate in a ring near the LS radius. One expects this to be the case for dwarf novae, for example. There are indications that in T CrB the gM3 star may have a roughly constant mass transfer rate of $\sim 10^{-6}$ $M_{\odot}$ yr^{-1} (Kenyon 1986). One anticipates such a value for systems which are in the early stages of unstable runaway mass transfer (i.e., wherein the mass of the loser exceeds that of the gainer). We may provide a simple estimate of the steady state accretion disk mass which would be sustained by this mass flux. Using equation (A3) of Cannizzo & Reiff (1992), which gives Σ as a general function of Ω, α, and $\dot{M}$, assuming $\alpha \sim 1$, $\dot{M} \sim 10^{-6}$ $M_{\odot}$ yr^{-1}, and $r_{disk} \sim 10^{12}$ cm—and taking a representative opacity law for the hot state $\kappa = 2.8 \times 10^{24}$ cm^2 g^{-1} $\rho T^{-3.5}$—we may integrate Σ over the disk to find $M_{disk} \sim 10^{-7}$ $M_{\odot}$. This is much less than the mass of the blob. A key ingredient in the rapid spreading of the blob is that it is able to come close to the accreting star on the first few periastron passages and feel the large tidal force there. Because it is not necessary to plow through a lot of preexisting disk material, this appears feasible. Since we neglect cooling, our precise esti-

mate of the rate of spreading may be too high; nevertheless it is probably unphysical for the gas to cool significantly below the temperatures characteristic of the envelope of the mass-losing star where the blob originated. Given the number of orbital timescales near the accreting star that must elapse between the two observed maxima, the gas temperature would have to be extremely small to prevent radial spreading due to gas pressure. It is also unfortunate that we are unable to compute a light curve directly for the primary maximum. As discussed earlier, this would be enormously difficult to do within a fully three-dimensional computation such as we have, since it would involve an immense radiative transfer calculation.

Our revised understanding of the blob physics led us to reexamine the spreading torus model of CK. The main finding of CK was that it was necessary to have the accretion disk viscosity parameter α increase exponentially with time to obtain the relatively fast rise and decay times required for the secondary maximum. Since their initial torus was concentrated at a single radius, they took for simplicity a unique growth rate timescale for α. In our current scenario we have a radially extended configuration as our starting point, therefore we must take into account a range in growth timescales. On physical grounds this seems plausible: since the viscous dissipation couples to the local orbital shear, the inner regions should approach the saturation value of α sooner than the outer regions. In a more fully self-consistent time-dependent disk computation one might also envisage a radial coupling of the viscous dissipation mechanism so that the growth rates at adjacent radii are not entirely independent of each other, but the correlation length involved in such a scenario would represent yet another free parameter (which is best avoided at the present level of sophistication). Within the paradigm of an exponentially increasing α, we were guided by the choices for the initial and final values of α_i and α_f determined empirically by CK. Again, if we had a complete theory for the viscosity, we could in principle prescribe values for α_i and α_f as functions of radius. Lacking such a theory, we take them to be constant. The saturation value α_f is set by the observed rate of decay of the secondary maximum to be ~ 3. By taking the local growth rate to be $\sim\Omega$ (i.e., $t_{\rm grow} \sim 1/\Omega$) we require $\alpha_i \sim 10^{-6}$ to $\sim 10^{-5}$. The effect of taking α_i smaller than the value adopted by CK (i.e., 0.001) is to decrease the rise time of the secondary maximum (measured backwards from the visual peak to the point roughly 2 mag below the peak) to $\sim$20–30 days—about the observed value. Since we now have substantial surface density at small radii in the early stages, there is an earlier contribution to the accretion luminosity than before. The pre-maximum light is now expected to be within about 2 mag of the peak visual brightness for a substantial fraction of the intermaximum interval. This level is comparable to the contribution from the gM3 mass loser. This may be an embarrassment for the present scenario, or it may simply reflect a failure of the blackbody assumption for the flux distribution of the disk. In addition, since our starting mass is in general higher than the masses employed by CK, we find the peak brightness to be greater. This may imply that T CrB is more edge-on than the 70° adopted by CK (which might be excluded by the lack of eclipses), or that our method of computing the visual flux from the disk is too crude.

An exponentially increasing α which grows at a rate given by the local Keplerian angular speed has interesting consequences for the evolution of the disk during the early stages. The high-viscosity matter in the inner disk tries to expand into the low-viscosity disk matter lying farther out, and this produces a local enhancement in $\Sigma(r)$ and $T(r)$ which travels outward at ~ 4 km s^{-1} for the parameters adopted in our modeling. Outside of this expanding ripple there is another transition front which is akin to the heating front found in dwarf novae. It represents a transition between the two branches of stable solutions which produce the S-curve in computations of the vertical accretion disk structure. Thus we have hot, ionized gas lying at small radii and cool, neutral gas at large radii. Whereas in dwarf novae the heating (and cooling) transition is brought about by the evolution of the surface density with respect to fixed critical surface densities, in the present situation we have just the opposite, i.e., a constant surface density in the disk during the early evolution but continually changing critical surface densities by virtue of the variation of α with radius and time. In our computations the α-wave lies interior to the ionized/neutral transition, and the α's corresponding to the two transitions are $\sim 10^{-1.5}$ and $\sim 10^{-4.0}$, respectively. Although in our models the ionized/neutral transition leads the α-wave by a factor of 2–3 in radii, we expect that a more detailed computation would show the two to be roughly coincident. There are two reasons for this: (1) The appropriate velocity for the ionized/neutral front (given by Meyer 1984, for example) is much slower than what we find in an overly simple model (given our local values for α and h/r). A self-regulating mechanism would, however, tend to nullify differences between the speeds of the two fronts by bringing the ionized/neutral interface farther upstream into disk matter with a larger α. (2) The critical surface densities in our vertically averaged time-dependent model underestimate the critical surface densities by ~ 10. This is equivalent to saying that the α corresponding to the critical surface density which equals the (fixed) surface density in the protodisk is overestimated by about the same factor. Therefore, the actual transition between ionized and neutral gas should lie farther upstream (i.e., at smaller radii) in matter which has been undergoing Keplerian shear for more local orbital times since $t = 0$ and hence possesses a larger value of α. Correcting for this effect in a completely self-consistent computation might reduce the brightness of the system during the $\sim$100 day interval before secondary maximum and thus bring the accretion luminosity to a lower value, more in accord with observations.

4. CONCLUSIONS

T CrB appears to be unique among objects with accretion disks in that we are able to observe the results of the finite time required for the viscous dissipation to become active, assuming that it couples to the local orbital shear as envisioned. We have shown, using a three-dimensional hydro computation, that the blob of matter proposed by Webbink (1976) to account for the primary maximum would become very spread out after its first few periastron passages around the secondary star and would probably have close to a flat surface density distribution within several dynamical times. (The lack of any strong shocks in our model would seem to argue against the mass accretion model for the outburst, because in the model it is the circularization of the torus which produces the primary maximum. We stress, however, that the preperiastron smearing may be caused to some extent by artificial viscosity.) Thus the starting point for an accretion disk model is a configuration in which $\Sigma(r)$ is constant within the Roche lobe of the accreting star. Using a one-dimensional hydro model for the accretion disk, we find that, during the early stages of its evolution, the high-viscosity

material in the inner regions attempts to spread out into the lower viscosity disk. This "α-wave" propagates a ripple in the surface density and also promulgates continuously changing critical surface densities which separate the ionized and neutral portions of the disk. This leads to a heating transition front (like that in dwarf nova accretion disks) which lies downstream from the α-wave. Although the speeds of the two fronts are not in general equal, a self-regulating mechanism would move the heating front into material with an α which would ensure that $v_F(\alpha) = v_\alpha$, since the ultimate driving mechanism for both waves is the outward increase in α brought about by our assumption $t(\alpha) \propto 1/\Omega$.

The light curves which we compute reproduce the observed light curve for the secondary maximum in the 1946 eruption. In our model the maximum occurs when the α-wave reaches the outer edge of the protodisk and the bulk of the matter begins to accrete. For our "standard model" the initial and saturation values for α are 10^{-5} and 3, respectively. As in CK, these values are in line with models for the viscous dissipation in which one starts from a "seed" value and ends with a state in which the medium that generates α (e.g., magnetic fields, turbulence) is in rough equipartition with the energy density of the gas. It may be a point of concern that in dwarf novae where one has fairly firm estimates of the α-values by comparing theory with observation within the context of the limit cycle model for outbursts, one gets $\alpha \sim 0.03$ for neutral disks and $\alpha \sim 0.1$ for ionized disks (Cannizzo, Shafter, & Wheeler 1988; Mineshige & Wood 1989). Since the accretion disks in these systems have existed for very many orbital timescales, these values for α should represent what we term α_f—the saturation value. There are several possibilities for this discrepancy: (1) It may be that α is a rather imperfect scaling for the viscosity. The fact that the dwarf nova accretion disks are ~ 100 times smaller than the one in T CrB could lead to a situation wherein equipartition of the viscous dissipation mechanism corresponds to $\alpha \sim 3$ for the large disk and yet $\alpha \sim 0.1$ for the smallest disks, i.e., a scaling of α_f with radius. (There might also be a scaling with h/r to give the difference between the two temperature states in dwarf novae; Meyer & Meyer-Hofmeister 1983.) (2) The parameter α is a good scaling for the viscosity, but there is some external agent that varies from system to system which mediates the rate of viscous dissipation, such as the mass-losing star. This could be enacted through the tidal torque or a magnetic field which would interact with the outer accretion disk edge. (3) The physical mechanism for viscous dissipation is different in different systems. It could be that a variety of physical mechanisms exist in nature for transporting material in accretion disks, and the specific mechanism for which a particular disk opts is determined by the length scales and other specifics of that given system. Given the rather wide range of physical systems in which accretion disks are thought to reside, this last possibility may be at least as likely as the other two.

We acknowledge useful conversations with Henk Spruit, Friedrich Meyer, and Ron Webbink. We thank Hyung Mok Lee for improving the one-dimensional accretion disk code. J. K. C. acknowledges the support of the Alexander von Humboldt Foundation, the Max Planck Institute for Astrophysics, the National Academy of Sciences, and the Laboratory for Astronomy and Solar Physics at Goddard Space Flight Center.

REFERENCES

Bath, G. T., & Pringle, J. E. 1981, MNRAS, 194, 967
Cannizzo, J. K. 1992, ApJ, 385, 94
Cannizzo, J. K., & Kenyon, S. J. 1992, ApJ, 386, L17 (CK)
Cannizzo, J. K., Lee, H. M., & Goodman, J. 1990, ApJ, 351, 38
Cannizzo, J. K., & Reiff, C. M. 1992, ApJ, 385, 87
Cannizzo, J. K., Shafter, A. W., & Wheeler, J. C. 1988, ApJ, 333, 227
Cannizzo, J. K., & Wheeler, J. C. 1984, ApJS, 55, 367
Colella, P., & Woodward, P. R. 1984, J. Comput. Phys., 54, 174
Evans, C. R., & Kochanek, C. S. 1989, ApJ, 346, L13
Hawley, J. F., & Balbus, S. A. 1991, ApJ, 376, 223
Hut, P., & Paczyński, B. 1984, ApJ, 284, 675
Kenyon, S. J. 1986, The Symbiotic Stars (Cambridge: Cambridge Univ. Press)
Kenyon, S. J., & Garcia, M. R. 1986, AJ, 91, 125 (KG)
Lubow, S. H., & Shu, F. H. 1975, ApJ, 198, 383 (LS)
Meyer, F. 1984, A&A, 131, 303
Meyer, F., & Meyer-Hofmeister, E. 1983, A&A, 128, 420
Mineshige, S., & Wood, J. H. 1989, MNRAS, 241, 259
Ruffert, M. 1992, A&A, 265, 82
Ruffert, M., & Müller, E. 1990, A&A, 238, 116
Selvelli, P. L., Cassatella, A., & Gilmozzi, R. 1992, ApJ, 393, 289
Webbink, R. F. 1976, Nature, 262, 271
Webbink, R. F., Livio, M., Truran, J. W., & Orio, M. 1987, ApJ, 314, 653